A Review of Perfectly Matched Absorbers for the Finite-Volume Time-Domain Method

T. Kaufmann, K. Sankaran, C. Fumeaux, and R. Vahldieck

Laboratory for Electromagnetic Fields and Microwave Electronics - IFH, ETH Zurich
Zurich, CH-8092, Switzerland, Email: thomas.kaufmann@ifh.ee.ethz.ch

Abstract **–** Different implementations of planar perfectly matched absorbers are studied under the unified framework of the Finite-Volume Time-Domain (FVTD) method. This comparative analysis allows to discuss the similarities existing between the theoretical models and explores the differences in their practical implementation and numerical performance in the framework of the FVTD method. Numerical experiments for performance analysis of the different PML models are conducted in terms of discretization and angle of incidence using waveguide models. The results are compared to theoretically expected values and to the first-order Silver Müller absorbing boundary condition.

I. INTRODUCTION

One of the biggest challenges in computational electromagnetics is to find domain truncation techniques which can accurately simulate an infinite space in a finite computational domain. The perfectly matched layer (PML) technique was introduced in [1] and it improved the accuracy of the numerical simulations by many orders of magnitude compared to previously applied traditional absorbing boundary conditions. Different implementations of the PML technique were reported in the literature giving rise to two general classes, namely non-Maxwellian (split) and Maxwellian (unsplit) absorbers. The implementation of the PML technique in conformal methods were limited to the Finite-Element Frequency-Domain or Time-Domain methods [2, 3]. A vertex-centered Finite-Volume Time-Domain (FVTD) model (variational approach) of the Bérenger PML (B-PML) was reported in [4] for scattering problems. Recently the authors introduced the cell-centered FVTD implementation of B-PML and modified Lorentz material-based PML (M-PML) techniques in [5, 6]. The generalized theory based perfectly matched layer (GT-PML) [7] and the complex frequency shifted perfectly matched layer (CFS-PML) [8, 9] were introduced for the FVTD method in [10]. The present paper extends the discussion on the unsplit perfectly matched layer (U-PML) model [11] and provides a more thorough performance evaluation. The theory of five different PML techniques, namely B-PML, M-PML, U-PML, GT-PML and CFS-PML, is studied under the unified FVTD framework and the numerical performance of the different PMLs is compared. The abbreviations are summarized in Table 1.

The paper is arranged as follows. In Sec. II some fundamentals on the FVTD method are given in a notation that will be used throughout this paper. Sec. III focuses on both the split and unsplit PML models. Derivations of the different PML models are summarized with respect to the FVTD implementation and analytical relations between the PML models are given. The computational cost is compared in Sec. IV. Numerical experiments are presented in Sec. V for the different PML models, including an investigation of evanescent wave absorption. The conclusion in Sec.VI summarizes the findings and emphasizes the practical application range for the different PML models.

Table 1. List of abbreviations of the different PML models used in this publication.

Bérenger PML	B-PML
Modified Lorentz Material-based PML	M-PML
Unsplit anisotropic PML	U-PML
Generalized Theory based PML	GT-PML
Complex Frequency Shifted PML	CFS-PML

II. FUNDAMENTALS OF THE FVTD METHOD

The FVTD method belongs to the general class of conformal time-domain methods. For the spatial discretization, the FVTD method employs unstructured polygons (typically tetrahedrons in 3D and triangles in 2D) which can model complex geometries using highly inhomogeneous meshes. Furthermore, curved boundaries can be modeled with high accuracy because stair-casing errors are avoided. Although this flexibility in spatial discretization is common to all conformal methods, the advantage of the FVTD method lies in the combination of an unstructured spatial discretization with an explicit time update. The method applied in this paper uses a cell-centered approach, hence field values at cell centers are updated by summing up the incoming and outgoing fluxes through each cell face. The update equation can be formulated as follows,

$$\partial_t \boldsymbol{U}_i = -\frac{1}{|A_i|}\sum_{k=1}^{f} |S_k|\alpha_i^{-1}\boldsymbol{\mathcal{F}}_{\boldsymbol{U}_k^*}\cdot\boldsymbol{n}_k - \boldsymbol{\mathcal{L}}_i \qquad (1)$$

where $\boldsymbol{U}_i$ denotes the cell-center field values at the *i*th cell, $|A_i|$ is the cell-volume, $|S_k|$ the area of the *k*th face and $\boldsymbol{\mathcal{F}}_{\boldsymbol{U}_k^*} \cdot \boldsymbol{n}_k$ the sum of the incoming and outgoing flux with the normal vector $\boldsymbol{n}_k$ perpendicular to the face [12]. The '*' in the subscript indicates that the computed flux-function across each face depends on the field quantities at the edge-center. A second-order accurate MUSCL algorithm is employed for spatial discretization. The field values at the face-center are approximated with the help of corresponding cell-center field values. For more information on the FVTD method, the reader is referred to [12]. Material properties of the cells are given in the diagonal matrix α_i and a loss term $\boldsymbol{\mathcal{L}_i}$ allows to include material losses. The latter term will be used in the present work to incorporate the PML models into the FVTD method.

In order to simplify the investigation, the setup in this paper relies on a formulation using a two-dimensional (2D) transverse electric (TE) form of the Maxwell system. The magnetic fields are assumed to be in the *xy*-plane and the electric-field is directed along the *z*-axis transverse with respect to the plane of propagation (*xy*-plane). Thus the field vector $\boldsymbol{U}_i$ and the material parameter α_i inside the ith cell become,

$$\boldsymbol{U}_i = \begin{pmatrix} H_{xi} \\ H_{yi} \\ E_{zi} \end{pmatrix} \quad \text{and} \quad \alpha_i = \begin{pmatrix} \mu_i & 0 & 0 \\ 0 & \mu_i & 0 \\ 0 & 0 & \varepsilon_i \end{pmatrix} . \quad (2)$$

For the time discretization, a second-order accurate explicit Lax-Wendroff scheme is employed which is based on a Predictor-Corrector algorithm [12]. There are other possibilities of time-stepping schemes such as the higher-order Runge-Kutta that can be employed within the presented framework. Although a 2D formulation is used here, the results can be generalized to 3D.

III. PERFECTLY MATCHED LAYERS

PMLs were first introduced for the Finite-Difference Time-Domain (FDTD) method by Bérenger in [13] using a non-Maxwellian split-field formulation. Later another class of approaches using a Maxwellian unsplit formulation was developed which includes M-PML [14], U-PML [11], GT-PML [7] and CFS-PML [8]. All variations were implemented in the FDTD method.

In the framework of the FVTD method the first-order Silver-Müller absorbing boundary condition (SM-ABC) is commonly used. However, the PML technique promises improved performance for off-normal incidence on the truncating boundary.

The theoretical discussions presented in this paper assume (without loss of generality) that all PML models are used to truncate the computational domain with a planar absorber along the y-direction and to absorb uniaxially along the x-axis (see Fig. 1). In future work these planar PMLs will serve as basis for generalization to conformal geometries such as cylinders [6] or spheres. Thus, corner regions are not considered in this publication.

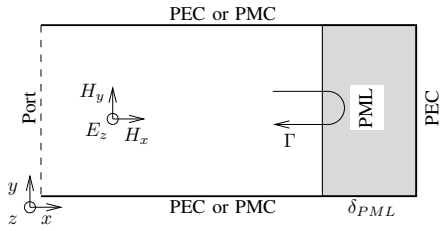

Fig. 1. Configuration of the uniaxial PML models in x-direction for the two-dimensional TE setup. The boundaries along the x-direction depend on the numerical experiment and are either PEC (rectangular waveguide) or PMC (parallel-plate waveguide).

A. Split PML

The Bérenger PML (also called the split-field PML) involves unphysical field splitting inside the PML domain which results in an increased number of update equations. For a complete theoretical treatment of the FVTD formulation of B-PML, refer to [5]. Due to the field splitting, an additional field component E_{zy} is introduced thus, expanding the field vector to $\boldsymbol{U}_i = [H_{xi}, H_{yi}, E_{zi}, E_{zyi}]^T$.

It is worth mentioning that in the above update equations, the fourth field equation for E_{zy} constitutes the non-hyperbolic part of the system and requires special treatment for its update. By employing the Rankine-Hugoniot jump relation discussed in [5], the field values of E_{zy} can be updated in a stable manner using the following flux term,

$$\mathcal{F}_{E_{zy}} \cdot n_k = \frac{n_y}{2}(H_{xl} + H_{xr}) - \frac{n_y^2}{2}(c_r \varepsilon_r E_{zr} - c_l \varepsilon_l E_{zl}) . \quad (3)$$

The loss vector $\boldsymbol{\mathcal{L}}_i$ used in the FVTD update equations for perfectly matched absorption is written as,

$$\boldsymbol{\mathcal{L}}_i = \begin{pmatrix} 0 \\ (\sigma_x/\varepsilon_i) H_{yi} \\ (\sigma_x/\varepsilon_i)(E_{zi} - E_{zyi}) \\ 0 \end{pmatrix} . \quad (4)$$

B. Unsplit PML

In order to avoid the unphysical additional field component, unsplit PML models have been developed based on anisotropic material properties. Those models still satisfy the Maxwell equations. For achieving uniaxial absorption in x-direction, the permittivity and permeability tensors are written as follows,

$$\overline{\overline{\varepsilon}} = \varepsilon\ [\Lambda],\ \overline{\overline{\mu}} = \mu\ [\Lambda] \quad \text{with} \quad [\Lambda] = \begin{pmatrix} 1/a & 0 & 0 \\ 0 & a & 0 \\ 0 & 0 & a \end{pmatrix} . \quad (5)$$

This form is derived under the condition of perfect matching as described in [7, 11, 14]. The four unsplit PML models presented in the following interpret this anisotropy matrix in different ways. In the case of

M-PML, the tensor describes a time-derivative Lorentz material model. In the case of U-PML the parameters are understood as physical material parameters which are included by explicitly using the magnetic and/or electric flux density. For GT-PML and CFS-PML, the matrix is interpreted as a complex coordinate stretching in frequency-domain which leads to integral or convolution terms in time-domain. In the following, update equations for the FVTD method are derived and compared theoretically.

1) Modified Lorentz Material-based PML - (M-PML): The idea of a modified Lorentz material-based absorber was introduced for the FDTD method in [14]. The anisotropy parameter a in this case is defined as $a = 1 + \chi_\omega^m$, with,

$$\chi_\omega^m = \frac{\omega_0^2[\chi_\alpha - j(\omega/\omega_0)\chi_\beta]}{\omega_0^2 - \omega^2 - j\Gamma\omega} \ . \tag{6}$$

The parameters χ_α, χ_β, Γ and ω_0 are chosen so that the material acts as a broadband absorber. The final system of update equations for the M-PML model can be written as,

$$\partial_t H_x = -\frac{1}{\mu}\partial_y E_z + \zeta H_x - G_x \tag{7}$$

$$\partial_t H_y = \frac{1}{\mu}\partial_x E_z - \zeta H_y, \tag{8}$$

$$\partial_t E_z = \frac{1}{\varepsilon}(\partial_x H_y - \partial_y H_x) - \zeta E_z, \tag{9}$$

$$\partial_t G_x = -\zeta G_x + \zeta^2 H_x, \tag{10}$$

where ζ is the material loss-parameter inside the absorbing layer. The fourth equation (10) is an ordinary differential equation in time and hence requires no special flux computation. Also the inherent structure of the Maxwellian system with three field components, namely H_x, H_y and E_z is preserved and there is only an auxiliary equation for the field component G_x which causes no significant computational overhead, in contrast to the B-PML model discussed in the previous section. The above system of equations is expressed in the FVTD method in notation (1) by defining the field vector as $\boldsymbol{U}_i = [H_{xi}, H_{yi}, E_{zi}, G_{xi}]^T$ and the corresponding PML loss vector $\boldsymbol{\mathcal{L}}_i$ as,

$$\boldsymbol{\mathcal{L}}_i = \begin{pmatrix} G_{xi} - \zeta H_{xi} \\ \zeta H_{yi} \\ \zeta E_{zi} \\ \zeta G_{xi} - \zeta^2 H_{xi} \end{pmatrix} \ . \tag{11}$$

The FVTD implementation of the M-PML adapted for unstructured grid is discussed in more detail in [6].

2) Unsplit anisotropic PML - (U-PML): Another approach to model unsplit PML based on the anisotropic material properties was introduced for the FDTD method in [11]. Using this model the component a in equation (5) is defined as

$$a = 1 + \frac{\sigma_x}{j\omega\varepsilon} \tag{12}$$

where σ_x represents the loss term and ε denotes the permittivity. In order to include this lossy frequency-domain parameter into the conformal time-domain update scheme, the physical magnetic flux density $\boldsymbol{B}$ is introduced (and/or the electric flux density $\boldsymbol{D}$, depending on the propagation mode). In the two-dimensional TE mode, the component of $\boldsymbol{B}$ in the anisotropy direction takes the form,

$$B_x = \frac{\mu}{1 + \frac{\sigma_x}{j\omega\varepsilon}} H_x \tag{13}$$

and needs to be explicitly included in the equation set because of its nonlinear frequency-dependence.

Based on [11], the following update equations can be derived,

$$\partial_t H_x = -\frac{1}{\mu}\partial_y E_z + \frac{\sigma_x}{\mu\varepsilon} B_x \tag{14}$$

$$\partial_t H_y = \frac{1}{\mu}\partial_x E_z - \frac{\sigma_x}{\varepsilon} H_y, \tag{15}$$

$$\partial_t E_z = \frac{1}{\varepsilon}(\partial_x H_y - \partial_y H_x) - \frac{\sigma_x}{\varepsilon} E_z, \tag{16}$$

$$\partial_t B_x = -\partial_y E_z \ . \tag{17}$$

In the FVTD formulation (1), the field vector $\boldsymbol{U}_i = [H_{xi}, H_{yi}, E_{zi}, B_{xi}]^T$ is then used. This leads to the following formulation for the FVTD method. The fourth flux term for the B_x field is identical to the flux of the H_x field ($\mathcal{F}_{B_x} = \mathcal{F}_{H_x}$) and hence, the PML loss vector becomes,

$$\boldsymbol{\mathcal{L}}_i = \begin{pmatrix} -\frac{\sigma_x}{\mu_i\varepsilon_i} B_{zi} \\ \frac{\sigma_x}{\varepsilon_i} H_{yi} \\ \frac{\sigma_x}{\varepsilon_i} E_{zi} \\ 0 \end{pmatrix} . \tag{18}$$

3) Generalized Theory based PML - (GT-PML): As opposed to the two previous approaches where the anisotropy tensor $[\Lambda]$ described a material property, the GT-PML model considers $[\Lambda]$ as a geometrical stretching operator ensuring perfect matching. In [7], the following complex frequency-dependant stretching factor is defined,

$$a = 1 + \frac{\omega_x''}{j\omega} \tag{19}$$

where ω_x'' describes the rate at which the field is attenuated within the PML. In the two-dimensional TE case, this leads to the usual lossy formulation for the electric field and the y-component for the magnetic field. In frequency-domain the x-component of the magnetic field becomes,

$$j\omega\mu H_x = -\partial_y E_z \cdot a = -\partial_y E_z - \frac{\omega_x''}{j\omega}\partial_y E_z \ . \tag{20}$$

Transforming this frequency-domain formulation into time-domain yields an integral term for the H_x-component and that results in the following GT-PML

update equations,

$$\partial_t H_x = -\frac{1}{\mu}\partial_y E_z - \frac{\omega_x''}{\mu}\int_0^t (\partial_y E_z)dt \quad (21)$$

$$\partial_t H_y = \frac{1}{\mu}\partial_x E_z - \omega_x'' H_y, \quad (22)$$

$$\partial_t E_z = \frac{1}{\varepsilon}(\partial_x H_y - \partial_y H_x) - \omega_x'' E_z \ . \quad (23)$$

In the notation of equation (1), the field vector for GT-PML is given as $\boldsymbol{U}_i = [H_{xi}, H_{yi}, E_{zi}]^T$ and the corresponding lossy PML vector for the FVTD method is,

$$\boldsymbol{\mathcal{L}}_i = \begin{pmatrix} -\frac{\omega_x''}{\mu_i}\int_0^t (\sum_{k=1}^f |S_k| \mathcal{F}_{H_{xk}^*} \cdot n_k)dt \\ \omega_x'' H_{yi} \\ \omega_x'' E_{zi} \end{pmatrix} \ . \quad (24)$$

4) Complex Frequency Shifted PML - (CFS-PML): The theory of CFS-PML was first introduced in [8] based on complex frequency shifted PML parameters. This shifting is a more general form of the factor used in the previous section, namely,

$$a = \kappa_x + \frac{\sigma_x}{\alpha_x + j\omega\varepsilon} \quad (25)$$

where κ_x represents the real geometrical stretching, α_x is used to control the absorption for evanescent waves and σ_x is the physical loss.

This approach is of particular interest for damping evanescent waves since all the conventional PML models described in the previous sections exhibit a performance degradation in the evanescent regime. The complex stretching factor described in [15] can be implemented in two ways. The first approach is using an auxiliary differential equation method and the second approach involves a time-domain convolution. For the present FVTD version of CFS-PML, the second approach is utilized. As shown in [9] this results in the following update equations,

$$\partial_t H_x = -\frac{1}{\mu}\partial_y E_z \kappa_x + \Psi_{H_x} \quad (26)$$

$$\partial_t H_y = \frac{1}{\mu}\frac{\partial_x E_z}{\kappa_x} - \frac{\sigma_x}{\varepsilon\kappa_x} H_y + \Psi_{H_y}, \quad (27)$$

$$\partial_t E_z = \frac{1}{\mu\kappa_x}(\partial_x H_y) - \frac{\sigma_x}{\varepsilon\kappa_x} E_z + \Psi_{E_z} \ . \quad (28)$$

Apart from the standard Maxwellian fields (H_x, H_y and E_z) and the material parameters ($\mu = \mu_r\mu_0$, $\varepsilon = \varepsilon_r\varepsilon_0$ and σ_x), two new factors, namely α_x and κ_x are introduced. These factors give additional degrees of freedom in controlling the perfectly matched damping behavior inside the PML. The terms Ψ_{H_x}, Ψ_{H_y} and Ψ_{E_z} in equations (26) to (28) represent the convolution operation in time for each field value and they can be written for the FVTD method as,

$$\Psi_{H_{xi}} = -\frac{\sigma_x}{\mu_i\varepsilon_i} e^{-\frac{\alpha_x}{\varepsilon_i}\cdot t} * \sum_{k=1}^{f} (\mathcal{F}_{H_{xk}^*} \cdot n_k)|S_k| \quad (29)$$

$$\Psi_{H_{yi}} = \frac{\alpha_x\sigma_x}{\kappa_x\varepsilon_i^2} e^{-\frac{\alpha_x}{\varepsilon_i}\cdot t} * H_{yi}, \quad (30)$$

$$\Psi_{E_{zi}} = \frac{\alpha_x\sigma_x}{\kappa_x\varepsilon_i^2} e^{-\frac{\alpha_x}{\varepsilon_i}\cdot t} * E_{zi} \ . \quad (31)$$

This describes the continuous-time formulation of the convolutions which would be highly inefficient to implement in a discrete-time scheme since a sum over all time needs to be calculated at each time step. Thus, the iterative method proposed in [9] can be applied to simplify the convolution to one addition per time step.

This formulation eventually allows to express a loss term using the field vector $\boldsymbol{U}_i = [H_{xi}, H_{yi}, E_{zi}]^T$ in equation (1) as,

$$\boldsymbol{\mathcal{L}}_i = \begin{pmatrix} -\Psi_{H_{xi}} \\ \frac{\sigma_x}{\varepsilon_i\kappa_x} H_{yi} - \Psi_{H_{yi}} \\ \frac{\sigma_x}{\varepsilon_i\kappa_x} E_{zi} - \Psi_{E_{zi}} \end{pmatrix} \ . \quad (32)$$

These convolution operations eventually make the CFS-PML highly efficient for the absorption of evanescent waves, however, at the cost of a somewhat increased computational effort.

Guidelines to choose the parameters are given in [16], where derivations show that the PML mainly absorbs propagating modes if the term $\frac{\sigma_x}{\alpha_x + j\omega\varepsilon}$ in equation (25) is mainly complex. In contrast, evanescent waves are best absorbed if the fraction is mainly real. Thus in the case of a waveguide the value for α_x has to be chosen so that the switching frequency,

$$f_\alpha = \frac{\alpha_x}{2\pi\varepsilon} \quad (33)$$

corresponds to the cutoff frequency. The factor κ_x stretches the coordinate system, which in practice affects the accuracy of the simulation. In the presented work κ_x is fixed at $\kappa_x = 1$ in order to avoid stretched coordinate discretization errors.

C. Relationships between PML models

1) Unsplit PML models: Comparing the formulations of M-PML, U-PML and GT-PML suggests a close similarity even though the approaches differ in their physical interpretations. M-PML and U-PML both use one additional field term and GT-PML incorporates an additional integral term. When rewriting the set of equations for M-PML (7) to (10) by inserting the additional field term $G_x = K_x + \zeta H_x$ into equation (7), the following set

emerges,

$$\partial_t H_x = -\frac{1}{\mu}\partial_y E_z - K_x \quad (34)$$

$$\partial_t H_y = \frac{1}{\mu}\partial_x E_z - \zeta H_y, \quad (35)$$

$$\partial_t E_z = \frac{1}{\varepsilon}(\partial_x H_y - \partial_y H_x) - \zeta E_z, \quad (36)$$

$$\partial_t K_x = \frac{\zeta}{\mu}\partial_y E_z, \quad (37)$$

where K_x represents the magnetic polarization current. Comparing the rewritten system in equations (34) to (37) of M-PML with that of U-PML in equations (14) to (17), their mathematical equivalence becomes apparent, although different physical quantities are considered (K_x and B_x).

Applying a similar reformulation of GT-PML, the integral term can be written as a separate update equation identical to the one of U-PML. This rewriting is required anyhow before numerical implementation to allow for the iterative integration. In the present formulation, the Lax-Wendroff time stepping is applied. This allows for sophisticated integration methods. In this case the Simpson rule is used because it fits perfectly into the two step updating scheme. Therefore the final numerical FVTD implementations of the three PML models differ slightly, albeit they are analytically equivalent. Hence, for the numerical implementation of the scheme only minor differences in the range of the numerical precision are expected.

The relationship between the absorption parameters used in the different formulations can be expressed as follows,

$$\zeta = \omega_x'' = \frac{\sigma_x}{\varepsilon}. \quad (38)$$

2) Split vs. Unsplit PML: Considering further the relation between split and unsplit models, a close connection can be found between B-PML and U-PML, as pointed out in [11, 17]. Splitting the U-PML formulation, the formulation for B-PML can be retrieved, or vice-versa. Hence, numerically identical results are expected here as well.

3) CFS-PML to GT-PML: Finally it has to be pointed out that, as CFS-PML is a generalization of GT-PML, the convolutions of equations (29) to (31) should reduce to the integral term of GT-PML if $\alpha_x \to 0$ and $\kappa_x = 1$. In fact it can be verified that,

$$\lim_{\alpha_x \to 0, \kappa_x = 1} \Psi_{H_{xi}} = -\frac{\sigma_x}{\mu_i \varepsilon_i} * \sum_{k=1}^{f} (\mathcal{F}_{H^*_{xk}} \cdot n_k)|S_k| \quad (39)$$

$$\lim_{\alpha_x \to 0, \kappa_x = 1} \Psi_{H_{yi}} = 0, \quad (40)$$

$$\lim_{\alpha_x \to 0, \kappa_x = 1} \Psi_{E_{zi}} = 0\ . \quad (41)$$

The convolution in equation (39) is a simple integration over time, and thus yields exactly the same term as in GT-PML. This also applies to the discrete formulation obtained by the method of [9]. Figure 2 summarizes the relationship between all the investigated PML models.

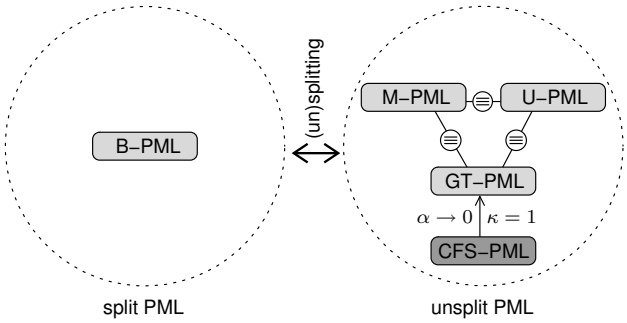

Fig. 2. Analytical relationship between the investigated PML models.

IV. CONSIDERATIONS ON COMPUTATIONAL EFFORT

It is shown in the previous section that the analytical formulations of B-PML, M-PML, U-PML and GT-PML are analytically equivalent. Nevertheless, the discrete models vary because of the different required operations. The numerical implementations include an additional flux term for B-PML, additional update equations for M-PML and U-PML and an integral term for GT-PML.

Table 2 shows the number of variables necessary for the investigated PML models in 2D. In free space only three field variables are updated using three flux terms. In the case of B-PML, the fourth split field requires the calculation of an additional flux term at each time step. This is not necessary for M-PML. Due to the nature of the fourth differential equation, no flux needs to be calculated, but one additional update equation is necessary. The fourth field in U-PML requires calculation of an additional flux. But since this flux is identical to the flux of the H_x field, that does not increase the computational cost. The formulation of GT-PML requires no additional update equation, and thus has only three field variables. In the numerical implementation however, the update formulation of the integral term leads to an additional variable, hence making the formulation identical to U-PML. Nevertheless the computational effort for GT-PML might increase depending on the sophistication of the

Table 2. Computational effort for two-dimensional models. K is the number of field update variables, M the number of flux variables and N the number of additional update variables.

Model	K	M	N	Auxiliary operation
free space	3	3	0	-
B-PML	4	4	0	flux
M-PML	4	3	0	ODE
U-PML	4	3	0	PDE
GT-PML	3	3	1	integral
CFS-PML	3	3	3	convolutions

integration method. Finally, CFS-PML adds a convolution operation to each field term, thus adding three additional operations and variables per cell in the two-dimensional TE case.

To summarize the computational effort necessary for all PML models, B-PML is slightly more costly than the basic unsplit PML models due to the calculation of the additional flux. CFS-PML significantly increases the computational costs as it requires one additional convolution operation for each field variable. In this case increased absorption for evanescent waves is achieved at the cost of increased memory and computation time.

V. NUMERICAL PERFORMANCE COMPARISON

To validate the theoretical findings of the previous section, numerical measurements are performed using first a plane wave problem and second a waveguide problem. These particular setups were chosen to measure the influence of discretization and to investigate the reflection at off-normal angles of incidence. As the implementation of U-PML and GT-PML are identical in FVTD, U-PML results are not displayed explicitly.

A. Plane Wave at Normal Incidence

At normal incidence the broadband performance of all the PML models is compared to that of the first-order SM-ABC. Broadband analysis provides information on the influence of the spatial discretization and the thickness of the absorbing layer in terms of the wavelength. A plane wave is simulated using a parallel-plate waveguide setup in Fig. 1 (with PMC boundaries). The scattering parameter extraction as discussed in [18] is used to retrieve the reflection coefficient S_{11} of the PML models. The results are shown in Fig. 3 with the PML parameters set to achieve a theoretical reflection [13] of $R = -80$ dB. The model is fed with a sine-modulated Gaussian broadband pulse with effective bandwidth stretching from 1 GHz to 50 GHz. It is observed that the PML performance over the whole bandwidth remains close to the theoretically expected value, with a degradation at higher frequencies due to coarse spatial discretization. In the investigated problem, the overall performance of the SM-ABC is inferior to that of the PML models over most of the frequency range. At low frequencies (fine spatial discretization) the influence of discretization errors diminishes. It is noticed that the performance of SM-ABC at normal incidence numerically converges towards perfect absorption.

It is observed that all the investigated PML models perform identically, as expected from the discussion in the previous sections. In particular in the present configuration CFS-PML becomes numerically and theoretically identical to GT-PML. This is due to the fact that the parallel plate waveguide exhibits a cutoff frequency $f_c = 0$ and thus, according to equation (33) $\alpha_x = 0$. Consequently the CFS-PML model becomes identical to GT-PML.

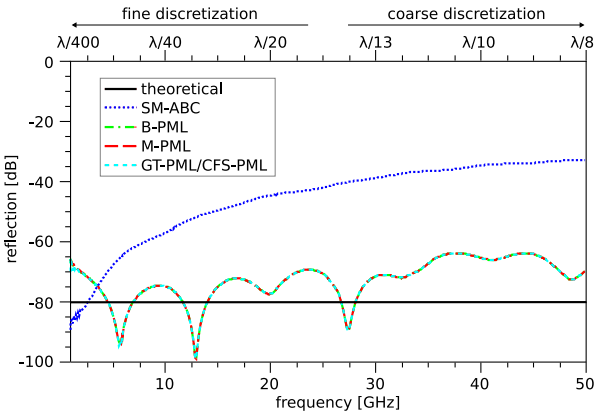

Fig. 3. Numerical results at normal incidence. The spatial discretization is shown in the upper scale.

B. Off-Normal Incidence and Evanescent Waves

In the second example, a waveguide model (Fig. 1 with PEC boundaries) excited with a TE_{10} mode is used to compute the reflection coefficient of the investigated PML models at a range of incident angles. In addition this model permits evaluation of absorption below the cutoff frequency of the waveguide, i.e., for evanescent waves. To measure the reflection of evanescent waves, the technique introduced by Gwarek et al. in [19, 20] is applied here to extract the S_{11}-parameter. This technique uses the tangential fields (E_z and H_y) and gives information on the physical reflection of the fields, even for evanescent waves. This stands in contrast to the traditional definition of scattering parameters based on the energy flow, where evanescent waves are understood to be totally reflected.

The investigated model has a cutoff frequency of 6.56 GHz for its fundamental TE_{10} mode and is fed with a modulated Gaussian broadband pulse with bandwidth stretching from 4 GHz to 20 GHz which spans both the evanescent and propagation regions. The spatial discretization employed for the model corresponds to a range of $\lambda/20$ to $\lambda/100$ (free-space wavelength) at the highest and lowest frequency components of the input signal, respectively. Simulated PML models are B-PML, M-PML, GT-PML and CFS-PML which are compared to the performance of the SM-ABC.

The results obtained are plotted in Fig. 4 with a theoretical reflection coefficient set to $R = -80$ dB at normal incidence. Depending on the frequency, evanescent waves naturally decay inside the finite thickness of the PML. This influence is included in the depicted theoretical absorption below cutoff. Because the field pattern within a waveguide can be understood as a superposition of two plane waves travelling with a certain off-normal angle, the influence of the angle of incidence is also addressed in this experiment. The cutoff frequency corresponds to grazing incidence and at higher frequencies, the angle of incidence converges towards normal incidence. This angle is also given in the upper scale of Fig. 4 for illustration.

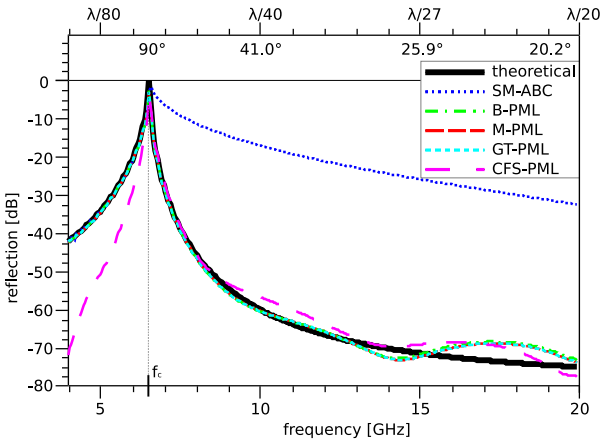

Fig. 4. Numerical results for off-normal incidence and evanescent waves in a waveguide model with thickness $a = 22.86$ mm. The upper scale shows the spatial discretization and the angle of incidence.

It is clearly noticed that above cutoff, all PML models perform very close to the theoretically expected value. Additionally it should be noted that the B-PML, M-PML and GT-PML models perform identically, as it was expected from their theoretical identity. Below cutoff, all ABCs except CFS-PML do not absorb and therefore only the natural decay is measured. In contrast, in the case of CFS-PML, the coordinate system stretching elongates the layer and hence the decay of evanescent waves is increased. This leads to an additional absorption of up to 30 dB in this case.

VI. CONCLUSION

In the present study different PML techniques were modeled in the unified framework of the FVTD method. The theoretical equivalence of M-PML, U-PML and GT-PML was discussed. Conditions were given that simplify CFS-PML to GT-PML. Numerical performances of all the PML models were found to be nearly identical for propagating modes. As expected, the performance of the CFS-PML was substantially better in the evanescent wave region compared to other PML models.

The improvement for CFS-PML compared to the other PML models arises for the absorption of evanescent waves and is achieved at the cost of an increased computational load. Therefore a practical application for the more costly model is only reasonable when strong evanescent waves have to be absorbed close to a source. Nevertheless the more efficient unsplit maxwellian PML models, such as the U-PML, are sufficient for most applications in conformal time-domain methods.

Although the results presented here were obtained employing planar perfectly matched layers, this study represents a first step towards the extension of PML techniques for non-planar surfaces in the FVTD method.

ACKNOWLEDGEMENT

This work is supported by the ETH Research Grant TH-38/04-1

REFERENCES

[1] J.-P. Bérenger, "A perfectly matched layer for the absorption of electromagnetic waves," *Journal of Computational Physics*, vol. 114, no. 2, pp. 185–200, 1994.

[2] Z. Sacks, D. Kingsland, R. Lee, and J.-F. Lee, "A perfectly matched anisotropic absorber for use as an absorbing boundary condition," *IEEE Transactions on Antennas and Propagation*, vol. 43, no. 12, pp. 1460–1463, December 1995.

[3] T. Rylander and J.-M. Jin, "Perfectly matched layer in three dimensions for the time-domain finite element method applied to radiation problems," *IEEE Transactions on Antennas and Propagation*, vol. 53, no. 4, pp. 1489–1499, April 2005.

[4] F. Bonnet and F. Poupaud, "Bérenger absorbing boundary condition with time finite-volume scheme for triangular meshes," *Applied Numerical Mathematics*, vol. 25, no. 4, pp. 333–354, December 1997.

[5] K. Sankaran, C. Fumeaux, and R. Vahldieck, "Cell-centered finite-volume based perfectly matched layer for time domain Maxwell system," *IEEE Transactions on Microwave Theory and Technique*, vol. 54, no. 3, pp. 1269–1276, March 2006.

[6] ——, "Uniaxial and radial anisotropy models for finite-volume Maxwellian absorber," *IEEE Transactions on Microwave Theory and Technique*, vol. 54, no. 12, pp. 4297–4304, December 2006.

[7] L. Zhao and A. Cangellaris, "GT-PML: Generalized theory of perfectly matched layers and its application to the reflectionless truncation of finite-difference time-domain grids," *IEEE Transactions on Microwave Theory and Techniques*, vol. 44, no. 12, pp. 2555–2563, December 1996.

[8] M. Kuzuoğlu and R. Mittra, "Frequency dependence of the constitutive parameters of causal perfectly matched absorbers," *IEEE Microwave Guided Wave Letters*, vol. 6, pp. 447–449, December 1996.

[9] A. Roden and S. Gedney, "Convolution PML (CPML): an efficient FDTD implementation of the CFS-PML for arbitrary media," *Microwave and Optical Technology Letters*, vol. 27, no. 5, pp. 334–339, 2000.

[10] K. Sankaran, T. Kaufmann, C. Fumeaux, and R. Vahldieck, "Different perfectly matched absorbers for conformal time-domain method: A finite-volume time-domain perspective," in *23rd Annual Review of Progress in Applied Computational Electromagnetics (ACES), Verona, Italy*, March 2007.

[11] S. Gedney, "An anisotropic perfectly matched layer-absorbing medium for the truncation of FDTD lattices," *IEEE Transactions on Antennas and Propagation*, vol. 44, no. 12, pp. 1630–1639, December 1996.

[12] P. Bonnet, X. Ferrieres, B. Michielsen, P. Klotz, and J. Roumiguiéres, *Time Domain Electromagnetics*. S. M. Rao, Ed., Academic Press, 1997, ch. 9, pp. 307–367.

[13] J.-P. Bérenger, "Three-dimensional perfectly matched layer for the absorption of electromagnetic waves," *Journal of Computational Physics*, vol. 127, no. 2, pp. 363–379, September 1996.

[14] R. W. Ziolkowski, "The design of Maxwellian absorbers for numerical boundary conditions and for practical applications using engineered artificial materials," *IEEE Transactions of Antennas and Propagation*, vol. 45, no. 4, pp. 656–671, April 1997.

[15] W. C. Chew and W. H. Weedon, "A 3D perfectly matched medium from modified Maxwell's equations with stretched coordinates," *Microwave Optics*, vol. 114, no. 2, pp. 185–200, 1994.

[16] J.-P. Bérenger, "Application of the CFS PML to the absorbtion of evanescent waves in waveguides," *IEEE Microwave and Wireless Components Letters*, vol. 12, no. 6, pp. 218–220, 2002.

[17] S. Gedney, "Perfectly matched layer absorbing boundary conditions," in *The Finite-Difference Time-Domain Method*, A. Taflove and S. C. Hagness, Eds. Artech House Inc., 2005.

[18] D. Baumann, C. Fumeaux, and R. Vahldieck, "Field-based scattering-matrix extraction scheme for the FVTD method exploiting a flux-splitting algorithm," *Microwave Theory and Techniques, IEEE Transactions on*, vol. 53, no. 11, pp. 3595– 3605, 2005.

[19] W. K. Gwarek and M. Celuch-Marcysiak, "Wideband S-parameter extraction from FD-TD simulations for propagating and evanescent modes in inhomogeneous guides," *Microwave Theory and Technique, IEEE Transactions on*, vol. 51, no. 8, pp. 1920–1928, 2003.

[20] ——, "A differential method of reflection coefficient extraction from FDTD simulations," *IEEE Microwave and Guided Waves Letters*, vol. 6, no. 5, pp. 1920–1928, 1996.

Thomas Kaufmann received the M.Sc. degree in electrical engineering and information technology from ETH Zurich, Switzerland in 2007 and is currently working towards the Ph. D. degree at the same university in the Laboratory for Electromagnetic Fields and Microwave Electronics (IFH). His research interest includes computational electromagnetics for microwave circuits and antennas. Mr. Kaufmann spent half a year in Toronto, Canada during an internship at InvoDane Engineering in 2004 and an exchange semester at the Norwegian University of Technology (NTNU) in Trondheim, Norway in 2005.

Krishnaswamy Sankaran received the B.Eng. degree (with a first-class distinction) in electrical and electronics engineering from the University of Madras, Madras, India, in 2002, the M.Sc. degree in information and communication engineering from the University of Karlsruhe TH, Germany, in 2004, and is currently working toward the Ph.D. degree from the ETH Zurich, Zurich, Switzerland. From October 2003 to May 2004, he was a Research Trainee with the European Commission, Joint Research Centre, Ispra, Italy, where he was involved in the field of radar systems engineering and remote sensing. In June 2004, he joined the ETH Zurich, where he is currently with the Laboratory for Electromagnetic Fields and Microwave Electronics (IFH). His main research interests are numerical methods for solving EM field problems, computational physics, and applied mathematics. In January 2007, he was invited by the Isaac Newton Institute for Mathematical Sciences, University of Cambridge, Cambridge, UK. Mr. Sankaran is currently the Chair of the IEEE Student Branch Zürich. He was the recipient of a full postgraduate scholarship and he was one of the recipients of the 2006 Best Student Paper Award presented at the IEEE Microwave Theory and Techniques Society International Microwave Symposium, San Francisco, CA.

Christophe Fumeaux received the Diploma and Ph.D. degrees in physics from the ETH Zurich, Switzerland, in 1992 and 1997, respectively. From 1998 to 2000, he was a Post-Doctoral Researcher with the School of Optics, University of Central Florida, Orlando. In 2000, he joined the Swiss Federal Office of Metrology, Bern, Switzerland, as a Scientific Staff Member. Since 2001, he has been a Research Associate with the Laboratory for Electromagnetic Fields and Microwave Electronics (IFH), ETH, Zurich, Switzerland. During the Fall of 2005, he was a Visiting Scientist with the Laboratory of Sciences and Materials for Electronics, and of Automatic (LASMEA), University Blaise Pascal, Clermont-Ferrand, France. His current main research interest concerns computational electromagnetics in the time domain for numerical analysis of microwave circuits and antennas. Dr. Fumeaux has been the chairman of the IEEE Swiss Joint Chapter on Microwave Theory and Techniques, Antennas and Propagation, and EMC since January 2006. He was the recipient of the ETH Silver Medal of Excellence for his doctoral dissertation. He was the corecipient of the outstanding paper award of the Applied Computational Electromagnetics Society (ACES) in 2004.

Rüdiger Vahldieck received the Dipl.-Ing. and Dr.-Ing. degrees in electrical engineering from the University of Bremen, Bremen, Germany, in 1980 and 1983, respectively. From 1984 to 1986, he was a Post-Doctoral Fellow with the University of Ottawa, Ottawa, ON, Canada. In 1986, he joined the Department of Electrical and Computer Engineering, University of Victoria, Victoria, BC, Canada, where he became a Full Professor in 1991. During the fall of 1992 and the spring of 1993, he was a Visiting Scientist with the Ferdinand-Braun-Institute für Hochfrequenztechnik, Berlin, Germany. In 1997, he became a Professor of EM-field theory with the ETH Zurich, Zurich, Switzerland, and Head of the Laboratory for Electromagnetic Fields and Microwave Electronics (IFH) in 2003. His research interests include computational electromagnetics in the general area of electromagnetic compatibility (EMC) and, in particular, for computer-aided design of microwave, millimeter-wave, and opto-electronic integrated circuits. Since 1981, he has authored or coauthored over 300 technical papers in books, journals, and conferences, mainly in the field of microwave computer-aided design. Prof. Vahldieck is the past president of the IEEE 2000 International Zurich Seminar on Broadband Communications (IZS2000). Since 2003, he has been president and general chairman of the International Zurich Symposium on Electromagnetic Compatibility. He is a member of the Editorial Board of the IEEE TRANSACTIONS ON MICROWAVE THEORY AND TECHNIQUES. From 2000 to 2003, he was an associate editor for the IEEE MICROWAVE AND WIRELESS COMPONENTS LETTERS, and from July 2003 until the end of 2005, he was the editor-in-chief. Since 1992, he has served on the Technical Program Committee (TPC) of the IEEE Microwave Theory and Techniques Society (IEEE MTT-S) International Microwave Symposium (IMS), the IEEE MTT-S Technical Committee on Microwave Field Theory, and in 1999, on the TPC of the European Microwave Conference. From 1998 to 2003, he was the chapter chairman of the IEEE Swiss Joint Chapter on Microwave Theory and Techniques, Antennas and Propagation, and EMC. Since 2005, he has been president of the Swiss Research Foundation on Mobile Communications. He was the recipient of the J. K. Mitra Award of the Institution of Electronics and Telecommunication Engineers (IETE) (in 1996) for the best research paper in 1995 and was corecipient of the Outstanding Publication Award of the Institution of Electronic and Radio Engineers in 1983. He was the corecipient of the 2004 Applied Computational Electromagnetic Society (ACES) Outstanding Paper Award.